Journal of Solid State Chemistry 187 (2012) 51–57

Contents lists available at SciVerse ScienceDirect

Journal of Solid State Chemistry

journal homepage: www.elsevier.com/locate/jssc

Introduction of oxygen vacancies and fluorine into TiO_2 nanoparticles by co-milling with PTFE

Mamoru Senna [a,*], Vladimir Šepelák [b], Jianmin Shi [a], Benjamin Bauer [a], Armin Feldhoff [c], Vincent Laporte [d], Klaus-Dieter Becker [a]

[a] Institute of Physical and Theoretical Chemistry, Technische Universität Braunschweig, Braunschweig, Germany
[b] Institute of Nanotechnology, Karlsruhe Institute of Technology, Eggenstein-Leopoldshafen, Germany
[c] Institute of Physical Chemistry and Electrochemistry, Leibniz University Hannover, Hannover, Germany
[d] Interdisciplinary Centre for Electron Microscopy, Ecole Polytechnique Fédérale de Lausanne, Lausanne, Switzerland

ARTICLE INFO

Article history:
Received 22 August 2011
Received in revised form
6 December 2011
Accepted 26 December 2011
Available online 4 January 2012

Keywords:
Titania nanoparticles
Poly(tetrafluoroethylene)
Mechanochemical reaction
Oxygen vacancies
Oxidative decomposition

ABSTRACT

Solid-state processes of introducing oxygen vacancies and transference of fluorine to *n*-TiO_2 nanoparticles by co-milling with poly(tetrafluoroethylene) (PTFE) powder were examined by diffuse reflectance spectroscopy (DRS) of UV, visual, near- and mid-IR regions, thermal analyses (TG-DTA), energy-dispersive X-ray spectroscopy (EDXS), X-ray photoelectron spectroscopy (XPS), high-resolution transmission electron microscopy (HRTEM) and X-ray diffraction (XRD). The broad absorption peak at around 8800 cm^{-1} (1140 nm) was attributed to the change in the electronic states, viz. electrons trapped at the oxygen vacancies (Vo) and *d*–*d* transitions of titanium ions. Incorporation of fluorine into *n*-TiO_2 was concentrated at the near surface region and amounted to ca. 40 at% of the total fluorine in PTFE, after co-milling for 3 h, as confirmed by the F1*s* XPS spectrum. The overall atomic ratio, F/Ti, determined by EDXS was 0.294. By combining these analytical results, a mechanism of the present solid state processes at the boundary between PTFE and *n*-TiO_2 was proposed. The entire process is triggered by the partial oxidative decomposition of PTFE. This is accompanied by the abstraction of oxygen atoms from the *n*-TiO_2 lattices. Loss of the oxygen atoms results in the formation of the diverse states of locally distorted coordination units of titania, i.e. $TiO_{6-n}Vo_n$, located at the near surface region. This leads subsequent partial ligand exchange between F and O, to incorporate fluorine preferentially to the near surface region of *n*-TiO_2 particles, where local non-crystalline states predominate.

1. Introduction

Anion substitution in TiO_2 has been extensively studied, mainly in the interests of visible light responsive photocatalysts [1–7]. One of the possible routes for anion substitution is milling titania with some organic crystalline species (OCs) as anion sources [8–15]. In contrast to the synthetic processes in a vapor or liquid phase, co-milling oxide nanoparticles with OCs is a solvent free solid state process and carried out at room temperature without requiring sealing or atmospheric control of the reaction systems.

As we reported elsewhere [16], incorporation of anions by co-milling is regarded as a solid state ligand exchange. We have also studied associated mechanisms for the favorable chemical interaction between some drugs and inorganic excipients [17–21]. Those mechanochemical processes include a two-electron transfer route like an acid–base reaction, and a one-electron mechanism under the concept of radical recombination. Usually, they occur simultaneously [21,22]. Such a forced ligand exchange is significantly enhanced when the ligand field symmetry is imbalanced [23,24].

Co-milling an inorganic mixture, comprising acidic oxides like SiO_2 or TiO_2 with basic hydroxides like $Mg(OH)_2$ or $Ca(OH)_2$, gives rise to the precursors of the complex oxides [25–29]. These series of solid state processes could be rather straightforwardly explained by neutralization at the interface of dissimilar solids, liberating a water molecule and leaving a hetero bridging bond [27–29].

In the present study, we examine the solid-state processes at the interfacial region between nano-particulate *n*-TiO_2 and poly(tetrafluoroethylene) (PTFE) under mechanical stressing. Fluorine was chosen for two reasons, i.e. (i) due to the close proximity of the ionic radii of F^- (e.g. the effective value of the Shannon diameter, 133 pm [30]) to that of O^{2-} (140 pm), and (ii) its potential to functionalize titania toward photosensitivity [31,32], although any applicational studies are out of the scope of the present report. PTFE was chosen

* Corresponding author. Fax: +81 45 564 0950.
E-mail address: senna@applc.keio.ac.jp (M. Senna).

0022-4596/$ - see front matter © 2012 Elsevier Inc. All rights reserved.
doi:10.1016/j.jssc.2011.12.036

as an OC of fluorine source because of its availability of stable fine particulates. Emphasis is laid on the mechanisms of the solid state processes at the boundary between PTFE and *n*-TiO_2.

2. Experimental methods

2.1. Sample preparation

As starting materials, anatase nanoparticles (Toho Titanium, TA50, average particle size 20 nm) and finely divided PTFE (Sigma-Aldrich, $<1\,\mu m$) were used as-received. Mechanical stressing was performed by using a planetary mill (Fritsch, Pulverisette 7) with a 45 mL vial and 15 balls of 10 mm in diameter made from yttrium stabilized zirconia (YSZ). A mixture comprising 3 g TA50 and 0.3 g or 0.6 g PTFE was subjected to milling at 720 rpm for up to 3 h. The milling operation was carried out in a tightly sealed vial without evacuating or controlling the background gas. Annealing was carried out in air up to 300 °C for 1 h.

2.2. Characterization

The diffuse reflectance spectra (DRS) of milled powders were measured in most cases in the wavelength range between 300 nm and 800 nm using a UV–vis–NIR spectrometer (Perkin Elmer, Lambda 900) equipped with a Praying Mantis accessory (Harrick). In some cases, the range was extended to the near infrared region, i.e. to 3000 nm. Diffuse reflectance spectra were also observed with a high performance FTIR spectrometer (Brucker, Equinox 55) to further examine the chemical changes of the ingredients of the co-milling.

Thermal analysis (TG-DTA) was performed by Netzsch STA409, using a heating rate of 10 K/min in air. Elemental analysis was performed by energy dispersive X-ray spectroscopy (EDXS), using an EDAX Genesis 4000 attached to a scanning electron microscope (JEOL, JSM-6400). High-resolution transmission microscopy (HRTEM) was made at 200 kV using a field-emission instrument with small spherical aberration's constant Cs = 0.5 mm (JEOL, JEM-2100F – UHR). EDXS was calibrated by comparison with well crystallized TiO_2 microparticles (Alfa Aesar, 99.99%). Changes in the crystallographical properties were monitored by conventional X-ray diffractometry (Philips PW1820).

Anion incorporation was further examined by X-ray photoelectron spectroscopy (XPS). XPS data were collected with an Axis Ultra instrument (Kratos Analytical, Manchester, UK) under ultra-high vacuum condition ($<10^{-8}$ Torr) and using a monochromatic Al *K*α X-ray source (1486.6 eV) in the Surface Analysis Facility of the Interdisciplinary Centre for Electron Microscopy at EPFL. The emitted photoelectrons were sampled from a $700\times350\,\mu m^2$ area with a 90° photoelectron take-off angle. The adventitious carbon 1*s* peak was calibrated at 285 eV and used as an internal standard to compensate for any charging effects. Both curve fitting of the spectra and quantification were performed with the CasaXPS software, using relative sensitivity factors given by Kratos.

3. Results and discussion

3.1. Changes in the electronic spectra by co-milling

After milling a mixture comprising the white powders of titania and PTFE, its color turned rapidly into dark gray and then black with increasing milling time. Associated unique diffuse reflectance spectra are shown in Fig. 1. We recognize that the shift of the absorption edge occurs at the early stage of milling,

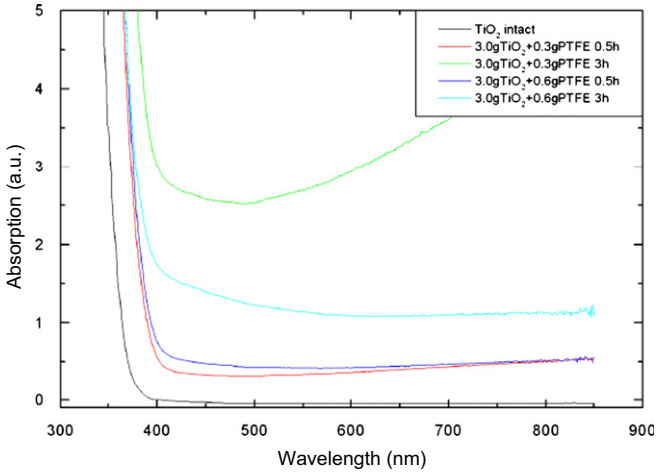

Fig. 1. UV–vis diffuse reflectance spectra of co-milled samples.

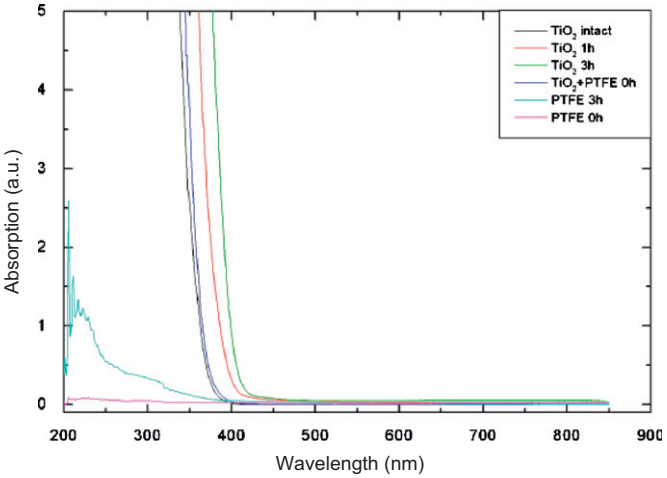

Fig. 2. UV–vis diffuse reflectance spectra of separately milled samples.

while the prolonged milling brings about a significant increase in the absorption intensity at lower energies in the visible and the near infrared (NIR) region. As the content of PTFE was increased from 10% to 20% of TiO_2, the absorption effect in the visible region was reduced. This is one of the typical mechanochemical phenomena, explained by the cushioning effect, i.e. the mechanical stress is reduced due to the increasing fraction of the soft ingredient, PTFE.

When titania or PTFE is milled separately, no spectral changes were observed, except for a slight shift of the absorption edge, in the case of titania, and a slight absorption in the UV range for PTFE, as shown in Fig. 2, although both samples appeared white to bare-eye inspection. Therefore, the absorption in the visible–NIR region, shown in Fig. 1, must be a consequence of the chemical interaction between titania and PTFE induced by the co-milling.

3.2. Introduction of oxygen vacancies

In the diffuse reflectance spectrum extended to the NIR region, a broad absorbance band peaked at around 8800 cm^{-1} (approx. 1140 nm, or 1.09 eV) was observed, as shown in Fig. 3. In view of the broadness of the observed electronic absorption band, there may be several ways of deconvolution, other than the one shown in Fig. 3. It is nonetheless recognized that there are components attributed to oxygen vacancies associated with F-type color centers [33], designated as peaks 1 and 2 at around 8000 cm^{-1}

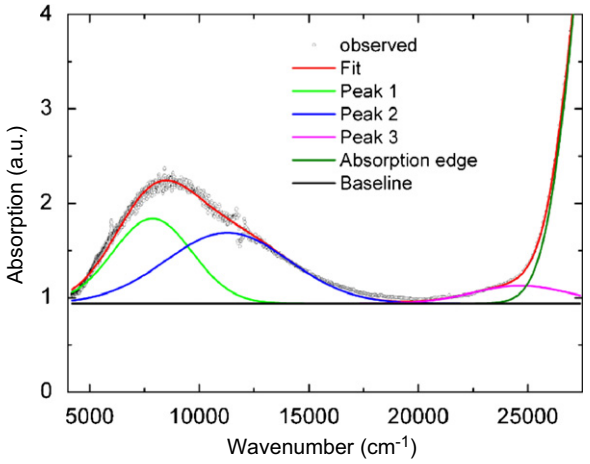

Fig. 3. UV–vis–NIR diffuse reflectance spectrum of the mixture co-milled for 3 h. Separated peaks 1 and 2 might be associated with oxygen vacancies with 1 and 2 electrons entrapped, while peak 3 is ascribed to *d*–*d* transition of Ti. See text for details.

and 11400 cm^{-1}, respectively. The band at about 24500 cm^{-1}, denoted as peak 3, is most probably attributed to *d*–*d* transition of Ti ions [34,35].

Based on a vast number of the published electronic absorption spectra of TiO_2, Kuznetsov et al. [36] concluded that the absorption peaks at photon energies below 2 eV are associated with electronic transitions involving various defects related to the reduction of titania [37]. Most of the absorption peaks in the visible to the NIR region are attributed to the intrinsic defects of TiO_2, irrespective of the incorporation or substitution of anionic species. The absorption edge shift observed in Fig. 2 can, therefore, be explained by the increased concentration of the defects created at the near-surface region of *n*-TiO_2 nanoparticles. The broadness of the absorption peak in Fig. 3 also indicates the diversity of the contributing electronic transition modes. This will further be discussed in Section 3.5.

3.3. Changes in the particle morphology

As shown in Fig. 4(a), the starting *n*-TiO_2 comprises fairly uniform cube-shaped particles of ca. 20 nm on the average. Higher magnification revealed well crystallized state including near surface region, see Fig. 4(b). After milling a mixture for 3 h, nanoparticles were partially disintegrated and severely agglomerated (Fig. 4(c)). Development of non-crystalline states in the near surface region extending up to 5 nm is also recognized upon higher magnification, as shown in Fig. 4(d). Note that mechanical stress-induced near surface amorphization less than 5 nm thick was observed even without any additives [38]. Therefore, the observed structural degradation in the near surface region is not necessarily the consequence of the mechanochemical reaction. These morphological changes are in line with the absorption edge shift mentioned in Section 3.2. Mechanical stress-induced surface destruction could reduce the effective electron mass due to the local decrease in the density and delocalize the electrons created by the reduction of the material, as the DFT study of Di Valentin et al. [39] implies, although the results based on the well defined models used in their DFT studies cannot directly be applied to the present case involving extensive lattice imperfections.

After annealing in air, absorption intensity extending to the NIR region was significantly reduced, while the absorption edge shift remained almost unchanged, as shown in Fig. 5. These spectroscopic observations suggest the partial annihilation of oxygen vacancies upon annealing in air. The slight shift of the

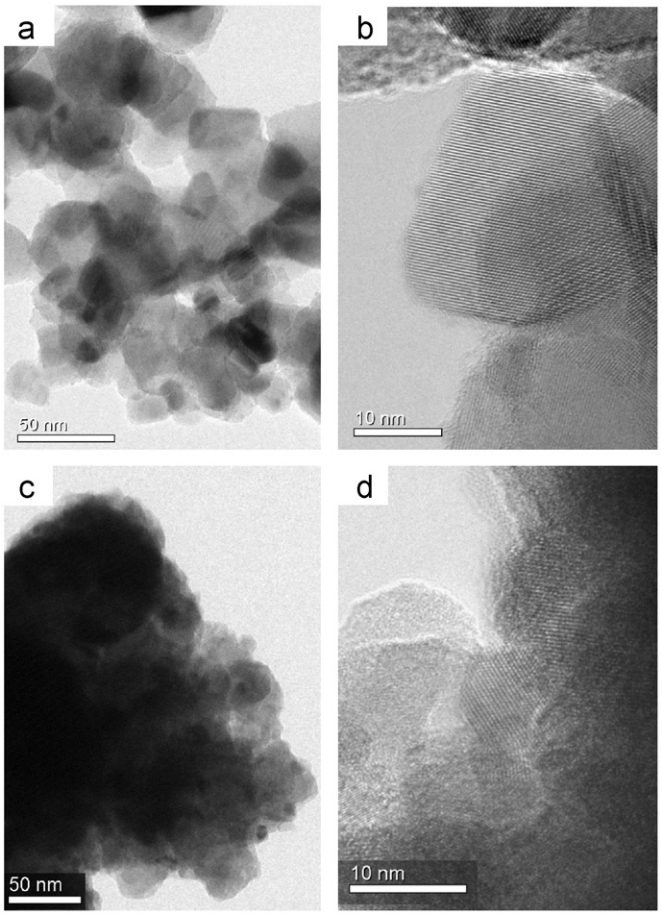

Fig. 4. Transmission electron micrographs: (a and b): intact *n*-TiO_2; (c and d): *n*-TiO_2 with 10 wt% PTFE, co-milled for 3 h.

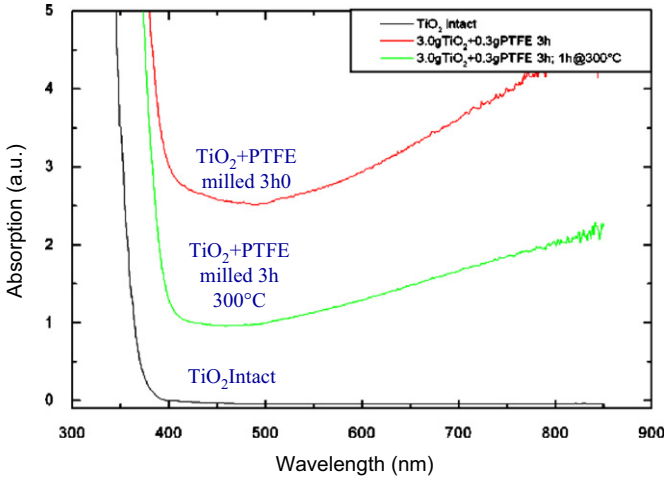

Fig. 5. UV–vis diffuse reflectance spectra of co-milled and annealed samples.

absorption edge toward higher energies is attributable to the partial recovery of the near surface disorder in *n*-TiO_2 [36].

3.4. Partial decomposition of PTFE

Representative infrared spectra of the system under study are shown in Fig. 6. In the pristine PTFE and its mixture with *n*-TiO_2 before co-milling, the typical signal of PTFE, i.e. symmetric and asymmetric C–F vibrational bands, are observed at around

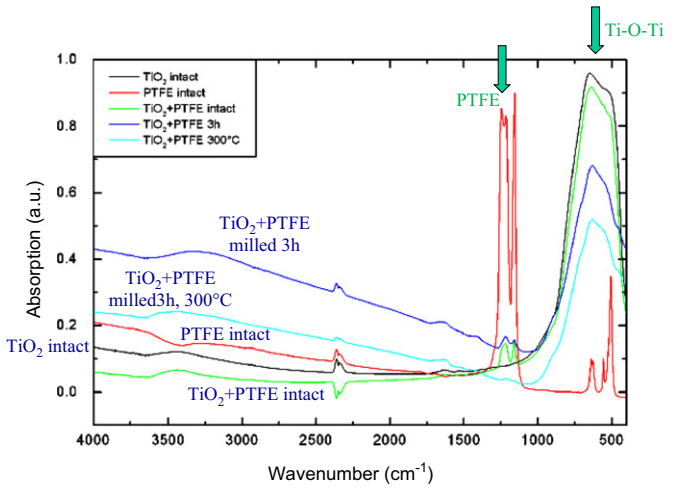

Fig. 6. Diffuse reflectance IR spectra of intact and co-milled samples.

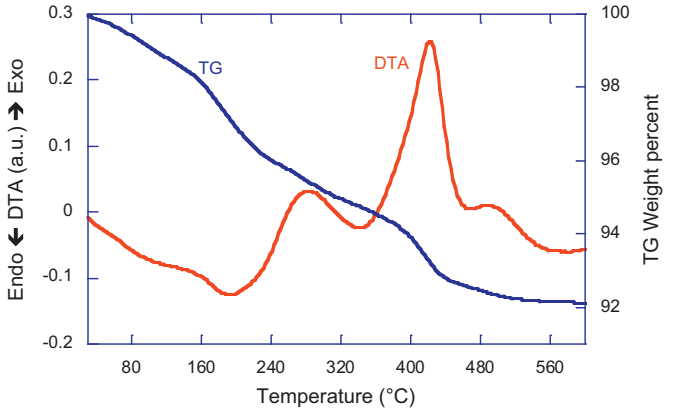

Fig. 7. TG-DTA profiles of n-TiO_2 with 10 wt% PTFE, co-milled for 3 h.

1200 cm^{-1} [40,41]. After co-milling, the intensity of these peaks, together with those ascribed to Ti–O and Ti–O–Ti vibrational bands at around 600 cm^{-1} [42], was reduced. The relative intensity of the band due to PTFE with reference to those of TiO_2 also was decreased. The latter indicates the dissociation of PTFE during milling in the presence of TiO_2. Indeed, we observed a surplus vial pressure as we opened the vial after milling, even after cooling down to room temperature. After annealing at 300 °C for 1 h in air, the PTFE peaks completely disappeared from the FTIR spectra. This is another indication of PTFE degradation during co-milling with TiO_2.

TG-DTA profiles of the sample n-TiO_2 with 10 wt% PTFE, co-milled for 3 h are shown in Fig. 7. The weight loss levels off at about 600 °C, where the total weight loss amounts to 7.8%. Since the starting mixture contained 9.1 wt% of PTFE, weight loss during co-milling was 14.0% of the total amount of PTFE in the initial mixture. We also note that the weight loss amounts to 5% by heating up to 322 °C, where the first exothermic process was completed. Since the pristine PTFE is much more stable, i.e. by heating in air at 465 °C for 1 h brings about a weight loss of about 1% [43], the severe degradation of PTFE by co-milling with TiO_2 is quite obvious from the thermal analysis as well.

3.5. *Incorporation of fluorine into titania*

Oxygen 1s XPS profiles shown in Fig. 8(a) are slightly shifted to higher energies after co-milling. The shift is in line with the transfer of electrons to the neighboring oxygen vacancies. We also

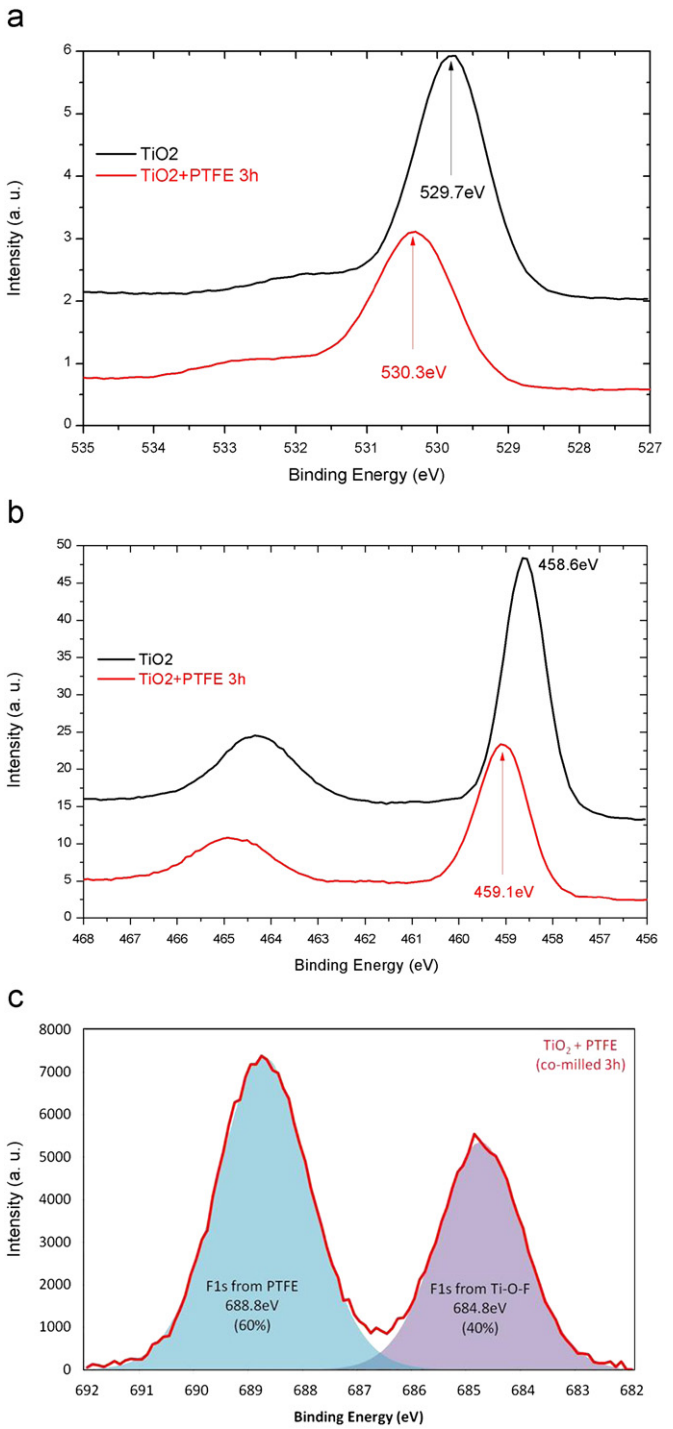

Fig. 8. XPS spectra of intact TiO_2 and co-milled samples: (a) O1s, (b) Ti2p and (c) F1s.

observed a similar shift for Ti2p, as shown in Fig. 8(b). This might suggest migration of electrons bound to oxygen and titanium ions toward oxygen vacancies, the latter serving as electron traps [44,45]. This tallies well with the observed DRS shown in Fig. 3. On the other hand, these shifts are also associated with the uptake of fluorine by n-TiO_2, as discussed below.

Independent of the spectral changes mentioned in Section 3.1, the chemical interaction between titania and PTFE is also verified by XPS analysis. As shown in Fig. 8(c), a new F1s peak appeared at around 685 eV after co-milling. Since this peak was not found in the pristine PTFE, as shown in Table 1, it must be ascribed to the

Table 1
Change in the XPS C1*s* and F1*s* by co-milling.

Sample	XPS signal relative intensity (%)						
	C1*s* 292 eV	C1*s* 290 eV	C1*s* 288 eV	C1*s* 286 eV	C1*s* 285 eV	F1*s* 689 eV	F1*s* 685 eV
PTFE	32				1	67	
TiO_2+PTFE co-milled[a]	11	12	10	4	11	31	21

[a] TA50+10 wt% PTFE after co-milling for 3 h.

product of the mechanochemical reaction of PTFE with *n*-TiO_2. The signal is similar to the one observed in $TiOF_2$ [46–49], so that we may reasonably conclude that fluorine has been incorporated into *n*-TiO_2, thereby changing its electronic states. Note that the relative XPS peak area of the new F1*s*, and hence the relative amount of fluorine incorporated from PTFE to the near surface region of *n*-TiO_2 particles, amounted to about 40%. While the XPS atomic ratio is restricted to the near surface region, the overall apparent atomic ratio F/Ti estimated by EDXS was 0.294. These results of XPS and EDXS are indicative of preferred accumulation of fluorine transferred from PTFE to the near surface region of titania, although quantitative discussion in this context is not possible at the present stage.

Electronic *d*–*d* transitions, suspected from the electronic spectra shown by peak 3 of Fig. 3, is often associated with Ti^{3+}, while we did not observe the corresponding XPS signal at around 457 eV [50]. It is well known, however, that forbidden electronic transitions like *d*–*d* or *f*–*f* turn partially to be allowed when the coordination symmetry is locally distorted. As a matter of fact, there are a number of phosphors whose photo- or electroluminescent properties rest upon those "forbidden" transitions [51,52]. Local distortion around Ti^{4+} is very likely to have taken place due to the introduction of oxygen vacancies and partial ligand exchange from oxygen to fluorine, e.g. the change from the octahedral coordination of TiO_6 to TiO_5F via TiO_5Vo or, more generally, $TiO_{6-n}Vo_n$. The very broad absorption peak shown in Fig. 3 is in line with the diversity of the $TiO_{6-n}Vo_n$ states, to be expected from the HRTEM image shown in Fig. 4(d). The apparent absence of a Ti^{3+} signal in XPS further suggests preferential incorporation of fluorine containing species from the oxidatively decomposed PTFE to fill the oxygen vacancies at the contact points to *n*-TiO_2.

3.6. Compositional and structural changes during co-milling

As shown in Fig. 2, milling titania separately brought about a negligible change in the color of the material. In contrast, co-milling with PTFE increased the absorption intensity in the visible region considerably. This is partly associated with electronic absorption due to oxygen vacancies as shown in Fig. 3 and discussed in Section 3.2.

As Kitahara et al. [53] reported, decomposition of PTFE in air produces various species including CF_2O, CF_3CFO, etc. They observed those oxidatively decomposed products in air at temperatures well above 400 °C. In our mechanochemical process, in contrast, the IR absorption peak from PTFE completely disappeared by annealing the co-milled products at 300 °C, as mentioned in Section 3.3. When we combine the observed destabilization of PTFE and the introduction of oxygen vacancies, it is reasonable to assume that partial oxidative decomposition of PTFE has taken place during co-milling with TiO_2, by abstracting oxygen ions.

According to the thermogravimetry shown in Fig. 7, 14% of PTFE was lost during co-milling, as mentioned in Section 3.4. The oxygen atoms needed for the oxidative decomposition of PTFE during co-milling can be preferentially supplied by the substrate, titania, which is forced to close contact with PTFE under mechanical stressing. The intake of oxygen from the ambient air in the vial may not categorically be excluded, but may be less probable, because the gaseous oxygen must be dissociated in order to trigger the oxidative decomposition of PTFE, whereas oxygen ions in the substrate titania are ready to transfer and are located immediately next to the PTFE surface. Possible participation of the radical species is yet to be examined.

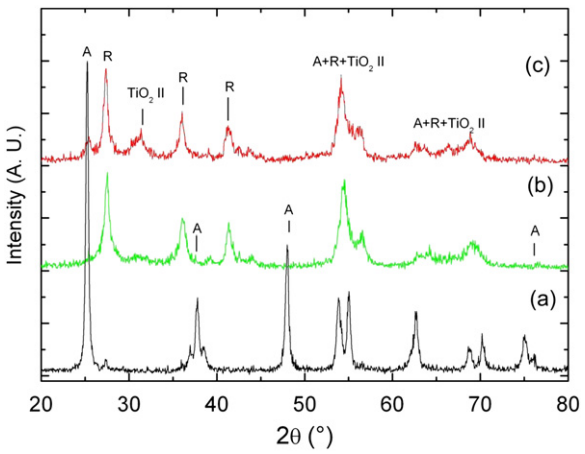

Fig. 9. X-ray diffraction profiles of TiO_2 milled with and without PTFE: (a) pristine TiO_2 (TA50), (b) TA50 milled for 3 h and (c) TA50 and PTFE co-milled for 3 h.

Carbon incorporation into *n*-TiO_2 due to the decomposition and fragmentation of PTFE during co-milling is also conceivable. As shown in Table 1, the C1*s* XPS signal of the milled mixture became much more manifold than that of pristine PTFE. The difference may be explained qualitatively by the coexistence of the decomposed fragments of PTFE. Detailed discussion of the decomposition products of PTFE and of the related possibility of carbon co-dope remain as open questions at this stage.

3.7. Mechanochemical processes at n-TiO_2/PTFE contact points

Once the partially decomposed PTFE is brought in intimate contact with the surface of *n*-TiO_2 nanoparticles, ligand exchange can easily occur, from the intact TiO_6 to TiO_5F [54,55] via $TiO_{6-n}V_{On}$. This process can be eased under mechanical stressing, where the long range ordering of the $TiO_{6-n}V_{On}$, units is severely disturbed, as shown in Fig. 4(d), and the atomic distances between Ti and F can become small enough for the fluorine atoms to enter into the ligand field of Ti. The XPS spectrum shown in Fig. 8(c) provides strong evidence for such a ligand exchange. A similar XPS profile was observed by Chiang et al. [56] in a TiO_2—poly (vinyldene fluoride) composite film.

As shown in Fig. 9, the changes observed in the X-ray diffractogram remain rather conventional. No appreciable peak shifts were

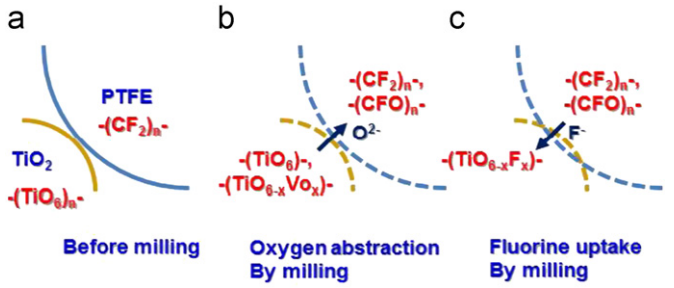

Fig. 10. Scheme of the reaction processes: (a) pristine mixture, (b) oxygen abstraction from TiO_2 and (c) fluorine migration from PTFE to TiO_2.

observed, indicating that fluorine transferred from PTFE to titania was confined at the near surface region, where the crystallinity was severely reduced, as shown in Fig. 4(d). The phase transformation from anatase to rutile induced by milling, which is revealed by the diffractograms is well documented [57,58]. Broad peaks of rutile are also explained conventionally by the small size of the crystallites. In contrast, the coexistence of a third phase, tentatively denoted as TiO_2-II, may need explanation. The TiO_2-II phase has been reported by Dachille et al. [59] as a high pressure phase. The appearance of high pressure phases during milling is frequently observed, see e.g. $CaCO_3$ [60] or PbO_2 [61]. Usually, this is also associated with the incorporation of impurities, which becomes even more appreciable when particle size is in the nanometer regime [62]. The appearance of the TiO_2-II phase in the present study may, therefore, be associated with the introduction of oxygen vacancies and the uptake of fluorine atoms.

As shown in Fig. 4(d), the disordered state of titania is restricted to the near surface region, within a few nanometers. The electron micrograph observation is in line with the X-ray diffractograms shown in Fig. 9, where no appreciable line broadening was recognized. Fig. 10 summarizes the proposed mechanisms of the present mechanochemical processes at the boundary between PTFE and *n*-TiO_2 nanoparticles.

Finally, we would like to mention the importance of introducing defects on the surface of titania, as Chen et al. [63] recently mentioned with the interests in the enhanced solar absorption. The mechanochemically modified *n*-TiO_2 in the present study is in line with their concept of disorder-engineered titania, although the application to the utilization of solar absorption of our modified titania nanoparticles is out of the scope of the present study.

4. Conclusions

By co-milling a mixture of *n*-TiO_2 and PTFE, significant amounts of oxygen vacancies were created in titania nanoparticles. Incorporation of fluorine into *n*-TiO_2 was concentrated at the near surface region and amounted to ca. 40 at% of the total fluorine in PTFE, after co-milling for 3 h, as confirmed by the F1*s* XPS spectrum. The overall atomic ratio, F/Ti determined by EDXS was 0.294. By combining these analytical results, a mechanism of the present solid state processes at the boundary between PTFE and *n*-TiO_2 was proposed. The entire process is triggered by the partial oxidative decomposition of PTFE. This is accompanied by the abstraction of oxygen atoms from the *n*-TiO_2 lattices. Loss of the oxygen atoms results in the formation of the diverse states of locally distorted coordination units of titania, i.e. $TiO_{6-n}Vo_n$, located at the near surface region. This leads subsequent partial ligand exchange between F and O, incorporate fluorine preferentially to the near surface region of *n*-TiO_2 particles, where local non-crystalline states predominate.

Acknowledgments

M.S. thanks Alexander von Humboldt-Foundation to enable his research stay in Braunschweig. V.S. thanks the DFG (SPP1415) for supporting this work. V.L. acknowledges N. Xanthopoulos (EPFL–Interdisciplinary Centre for Electron Microscopy) for performing XPS analyses. The authors thank Prof. B. Malic for TG-DTA measurement, and Toho Titanium Co. Ltd. for the kind donation of anatase nanoparticles, TA50.

References

[1] M.R. Hoffmann, S.T. Martin, W. Choi, D.W. Bahnemann, Chem. Rev. 95 (1995) 69–96.
[2] S. Sakthivel, H. Kisch, Angew. Chem. Intern. Ed. 42 (2003) 4908–4911.
[3] O. Diwald, T.L. Thompson, T. Zubkov, E.G. Goralski, S.D. Walck, J.T. Yates, J. Phys. Chem. B 108 (2004) 6004–6008.
[4] M. Sathish, B. Viswanathan, R.P. Viswanath, C.S. Gopinath, Chem. Mater. 17 (2005) 6349–6353.
[5] H. Wang, H.J.P. Lewis, J. Phys.: Condens. Matter 18 (2006) 421–434.
[6] M. Batzill, E.H. Morales, U. Diebold, Chem. Phys. 339 (2007) 36–43.
[7] H. Sun, S. Wang, H.M. Ang, M.O. Tade, Q. Li, Chem. Eng. J. 162 (2010) 437–447.
[8] S. Yin, H. Yamaki, M. Komatsu, Q. Zhang, J. Wang, Q. Tang, F. Saito, T. Sato, J. Mater. Chem. 13 (2003) 2996–3001.
[9] S. Yin, H. Yamaki, Q. Zhang, M. Komatsu, J. Wang, Q. Tang, F. Saito, T. Sato, Solid State Ionics 172 (2004) 205–209.
[10] S. Yin, H. Yamaki, M. Komatsu, Q. Zhang, J. Wang, Q. Tang, F. Saito, T. Sato, Solid State Sci. 7 (2005) 1479–1485.
[11] Y. Yamamoto, S. Moribe, T. Ikoma, K. Akiyama, Q. Zhang, F. Saito, S. Tero-Kubota, Molec. Phys. 104 (2006) 1733–1737.
[12] S. Yin, M. Komatsu, Q. Zhang, F. Saito, T. Sato, J. Mater. Sci. 42 (2007) 2399–2404.
[13] S. Livraghi, M.R. Chierotti, E. Giamello, G. Magnacca, M.C. Paganini, C. Cappelletti, C.L. Bianchi, J. Phys. Chem. C 112 (2008) 17244–17252.
[14] G. Liu, X. Wang, Z. Chen, M.M. Cheng, G.Q. Lu, J. Colloid Interface Sci. 329 (2009) 331–338.
[15] R. Rattanakam, S. Supothina, Res. Chem. Intermediates 35 (2009) 263–269.
[16] N. Tsuchiya, A. Tsukamoto, T. Ohshita, T. Isobe, M. Senna, N. Yoshioka, H. Inoue, Solid State Sci. 3 (2001) 705–714.
[17] T. Watanabe, S. Hasegawa, N. Wakiyama, F. Usui, A. Kusai, T. Isobe, M. Senna, J. Solid State Chem. 164 (2002) 27–33.
[18] T. Watanabe, S. Hasegawa, N. Wakiyama, A. Kusai, M. Senna, Int. J. Pharm. 248 (2002) 123–129.
[19] T. Watanabe, L. Ohno, N. Wakiyama, A. Kusai, M. Senna, S.T.P. Pharm. Sci. 12 (2002) 363–367.
[20] T. Watanabe, S. Hasegawa, N. Wakiyama, A. Kusai, M. Senna, Int. J. Pharm. 250 (2003) 283–286.
[21] T. Watanabe, N. Wakiyama, A. Kusai, M. Senna, Powder Technol. 141 (2004) 227–232.
[22] T. Watanabe, N. Wakiyama, A. Kasai, M. Senna, Ann. Chem. Sci. Mater. 29 (2004) 53–56.
[23] T. Ohshita, D. Nakajima, A. Tsukamoto, N. Tsuchiya, T. Isobe, M. Senna, Ann. Chem. Sci. Mater. 27 (2002) 91–101.
[24] T. Ohshita, K. Hisore, M. Komai, M. Senna, Syn. Reactivity Inorg. Metal-Org Nano-Metal Chem 25 (2005) 355–358.
[25] J.F. Liao, M. Senna, Thermochim. Acta 210 (1992) 89–102.
[26] J.F. Liao, M. Senna, Solid State Ionics 66 (1993) 313–319.
[27] T. Watanabe, J.F. Liao, M. Senna, J. Solid State Chem. 115 (1995) 390–394.
[28] T. Watanabe, T. Isobe, M. Senna, J. Solid State Chem. 122 (1996) 74–80.
[29] T. Watanabe, T. Isobe, M. Senna, J. Solid State Chem. 122 (1996) 291–296.
[30] R.D. Shannon, Acta Crystallogr. A32 (1976) 751–767.
[31] H. Sun, S. Wang, H.M. Ang, O. Moses, O. Tadé, L. Qin, Chem. Eng. J. 162 (2010) 437–447.
[32] S.N. Subbarao, Y.H. Yun, N.R. Kerfshaw, K. Dweight, A. Wold, Inorg. Chem. 18 (2010) 488–492.
[33] A.A. Lisachenko, V.N. Kuznetsov, M.N. Zakharov, R.C. Mikhailov, Kinetic Catal. 4 (2004) 189–197.
[34] K. Iijima, M. Goto, S. Enomoto, H. Kunugita, K. Ema, M. Tsukamoto, M. Ichikawa, H. Sakama, J. Lumin. 128 (2008) 911–913.
[35] K. Komaguchi, T. Maruoka, H. Nakano, I. Imae, Y. Ooyama, Y. Harima, J. Phys. Chem. C 114 (2010) 1240–1245.
[36] V.N. Kuznetsov, N. Serpone, J. Phys. Chem. C 113 (2009) 15110–15123.
[37] H. Skogby, U. Hålenius, P. Kristiansson, H. Ohashi, Am. Mineral. 91 (2006) 1794–1801.
[38] S. Indris, R. Amade, P. Heitjans, M. Finger, A. Haeger, D. Hesse, W. Gruenert, A. Boerger, K.D. Becker, Phys. Chem. B 109 (2005) 23274–23278.
[39] C. Di Valentin, G. Pacchioni, A. Selloni, J. Phys. Chem. C 113 (2009) 20543–20552.
[40] A.C. Rastogi, S.B. Desu, Polymer 46 (2005) 3440–3451.
[41] M. Kobayashi, M. Sakashita, T. Adachi, M. Kobayashi, Macromolecules 28 (1995) 316–324.

[42] B. Gao, Y. Ma, Y. Cao, W. Yang, J. Yao, J. Phys. Chem. B 110 (2006) 14391–14397.
[43] Sina Ebnesajjad, Fluoroplastics, Vol. 2: Melt Processible Fluoroplastics, Elsevier, Amsterdam, 2002, p. 12.
[44] A.C. Papageorgiou, N.S. Beglitis, C.L. Pang, G. Teobaldi, G. Cabailh, Q. Chen, A.J. Fisher, W.A. Hofer, G. Thornton, Proc. Natl. Acad. Sci. USA 107 (2010) 2391–2396.
[45] M.A. Henderson, W.S. Epling, C.H.F. Peden, C.L. Perkins, J. Phys. Chem. B 107 (2003) 534–545.
[46] G. Wu, J. Wen, S. Nigro, A. Chen, Nanotechnology 21 (2010). 085701/1-085701/6.
[47] D. Li, H. Haneda, S. Hishuta, N. Ohashi, Chem. Mater. 17 (2005) 2588–2595.
[48] H. Park, W. Choi, J. Phys. Chem. B 108 (2004) 4086–4093.
[49] Y. Wu, M. Xing, M.B. Tian, J. Zhang, F. Chen, Chem. Eng. J. 162 (2010) 710–717.
[50] H.L. Cai, X.S. Wu, J. Gao, Chem. Phys. Lett. 467 (2009) 313–317.
[51] T. Igarashi, M. Ihara, T. Kusunoki, K. Ohno, T. Isobe, M. Senna, J. Nanoparticle Res. 3 (2001) 51–56.
[52] W. Park, C.J. Summers, J. Mater. Sci. 37 (2002) 4041–4045.
[53] T. Kitahara, S. Takahashi, N. Kuramoto, M. Sala, T. Tsugoshi, M. Sablier, T. Fujii, Anal. Chem. 81 (2009) 3155–3158.
[54] E.A. Reyes-Garcia, Y. Sun, D. Raftery, J. Phys. Chem. C 111 (2007) 17146–17154.
[55] E.N. Anghel, P.- Florian, C. Bessada, J. Phys. Chem. B 111 (2007) 962–967.
[56] C.Y. Chiang, M.J. Reddy, P.P. Chu, Solid State Ionics 175 (2004) 631–635.
[57] J.M. Criado, C. Real, J. Soria, Solid State Ionics 32–33 (1989) 461–465.
[58] S. Begin-Colin, G. Le Caer, E. Barraud, O. Humbert, J. Mater. Sci. 39 (2004) 5081–5089.
[59] F. Dachille, P.Y. Simons, R. Roy, Am. Mineral. 53 (1968) 1929–1939.
[60] T. Isobe, M. Senna, J. Chem. Soc. Faraday Trans. I 84 (1988) 1199–1209.
[61] M. Senna, K. Schönert, Powder Technol. 31 (1982) 269–275.
[62] H. Liu, Z. Zheng, D. Yang, X. Ke, E. Jaatinen, J.C. Zhao, H. Zhu, ACS Nano 4 (2010) 6219–6227.
[63] X. Chen, L. Liu, P.Y. Yu, S.S. Mao, Science 331 (2011) 746–750.